Quantifying the stability of oxidatively damaged DNA by single-molecule DNA stretching

Micah J. McCauley[1], Leah Furman[2], Catherine A. Dietrich[3], Ioulia Rouzina[4], Megan E. Núñez[2] and Mark C. Williams[1,*]

[1]Department of Physics, Northeastern University, Boston, MA 02115, USA, [2]Department of Chemistry, Wellesley College, Wellesley, MA 02481, USA, [3]Department of Chemistry, Mount Holyoke College, South Hadley, MA 01075, USA and [4]Department of Chemistry and Biochemistry, The Ohio State University, Center for Retroviral Research, and Center for RNA Biology, Columbus, OH 43210, USA

ABSTRACT

One of the most common DNA lesions is created when reactive oxygen alters guanine. 8-oxo-guanine may bind in the *anti*-conformation with an opposing cytosine or in the *syn*-conformation with an opposing adenine paired by transversion, and both conformations may alter DNA stability. Here we use optical tweezers to measure the stability of DNA hairpins containing 8-oxoguanine (8oxoG) lesions, comparing the results to predictive models of base-pair energies in the absence of the lesion. Contrasted with either a canonical guanine-cytosine or adenine-thymine pair, an 8oxoG-cytosine base pair shows significant destabilization of several $k_B T$. The magnitude of destabilization is comparable to guanine-thymine 'wobble' and cytosine-thymine mismatches. Furthermore, the measured energy of 8oxoG-adenine corresponds to theoretical predictions for guanine-adenine pairs, indicating that oxidative damage does not further destabilize this mismatch in our experiments, in contrast to some previous observations. These results support the hypothesis that oxidative damage to guanine subtly alters the direction of the guanine dipole, base stacking interactions, the local backbone conformation, and the hydration of the modified base. This localized destabilization under stress provides additional support for proposed mechanisms of enzyme repair.

INTRODUCTION

8-oxoguanine (8oxoG) is a DNA damage product formed by the reaction of guanine bases with a variety of endogenous and exogenous oxidants (1–3). The 8oxoG lesion base is chemically similar to the normal guanine, differing only in the replacement of a hydrogen by oxygen at the C8 position and by protonation at the N7 position, both on the Hoogsteen edge of the base facing into the major groove (structures for G-C and 8oxoG-C are shown in Figure 1, and all others are shown in Supplementary Figure S1). Importantly, the 8oxoG lesion base retains guanine's flat, aromatic character and Watson–Crick edge, so the hydrogen bonds and stacking in the 8oxoG-cytosine base pair are highly similar to those in the undamaged G-C base pair (4,5). During replication, the 8oxoG lesion can be paired with adenine by high-fidelity replicative DNA polymerases (6,7). In the resulting 8oxoG-A pair, the 8oxoG base is flipped into the *syn* conformation, allowing it to form two hydrogen bonds with adenine and reducing the width of the purine–purine base pair (8). The effect of the 8oxoG-A base pair on DNA duplex stability is more severe than 8oxoG-C but less than a G-A mispair (9,10).

8oxoG is formed with facility in cells due to the leakage of reactive oxygen species from cellular respiration. In healthy human cells, the steady-state concentration is estimated to be around one 8oxoG per 10^6 guanines, representing a balance between rapid formation and robust removal (11). Repair is absolutely critical, since unrepaired 8oxoG-A base pairs will cause G to T transversion mutations after subsequent rounds of replication. Thus, 8oxoG is detected in the genome and repair is initiated by glycosylases such as the *Escherichia coli* enzyme MutM (Fpg) and the human enzyme hOGG1 as a part of the base excision repair system (BER) (12). These small enzymes quickly scan the DNA searching for the rare 8oxoG lesion and detect it efficiently despite that fact that 8oxoG differs from undamaged guanine by only two atoms. Once detected, the 8oxoG lesion is flipped out of the base pair stack and into the enzyme active site where the glycosidic bond is hydrolyzed. In a notable variation on the theme, the *E. coli* enzyme MutY corrects 8oxoG-A base pairs by specifically recognizing 8oxoG intra-helically but removing the misplaced adenine to prevent transversion mutations (13).

*To whom correspondence should be addressed. Tel: +1 617 373 5705 Fax: +1 617 373 2943; Email: mark@neu.edu
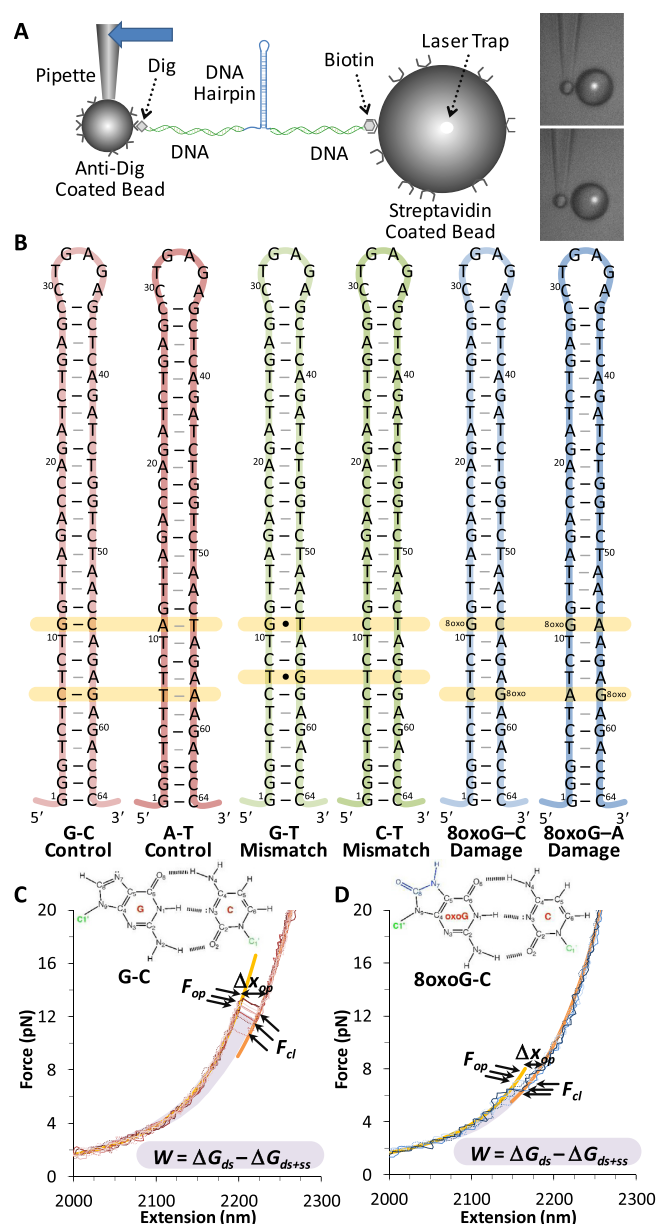
Figure 1. Probing the stability of non-canonical DNA. (**A**) Schematic for hairpin unzipping in optical tweezers experiments. Single hairpins are immobilized between two beads for fast force-ramp experiments. (**B**) Six hairpins compared in this study. Variations were made in the lower part of the stem (yellow bars). Control hairpins were fully matched including G-C and A-T pairs at the key sites (red backbones), which were replaced by G-T and C-T for the mismatched (green) and by oxidized guanine for the damaged 8oxoG-C and 8oxoG-A (blue). (**C**) Cycles of force extension (solid lines) and release (dotted lines) for fully matched hairpins (G-C at the key sites, shown inset). Five contiguous extension/release cycles (red) on the same hairpin display reproducible hairpin opening and closing. (**D**) Three cycles of 8oxoG-C containing hairpins (blue) show the destabilizing effect of oxidative damage (inset, with changes due to oxidative damage in blue). In both panels, the opening force (F_{op}), opening length (Δx_{op}) and closing force (F_{cl}) are identified for each cycle, between the modeled elasticities for the DNA handles (yellow) and the DNA handles plus the unfolded DNA (orange). These elasticities are quantified in the Supplementary Methods S2. The work of unfolding ($W = \Delta G_{ds} - \Delta G_{ds+ss}$) for a typical cycle is the area between these models (shaded violet).

The ability of BER glycosylases to distinguish between 8oxoG lesions and normal guanine as they scan rapidly along DNA is remarkable. The 8oxoG-C base pair does not distort the overall shape of the DNA to create a larger sign-post for damage nor does it open more frequently to solvent to enhance glycosylases' ability to 'catch' the lesion in an abundant extrahelical state (5,14,15). However, during the search process both MutM and hOGG1 'interrogate' the DNA by bending the backbone substantially and pushing on the edges of the base pairs from the minor groove (16–18). This localized application of stress has been proposed to destabilize selectively the 8oxoG-C base pair and lower the activation energy for extrusion and amino acid intercalation at 8oxoGC base pairs (19,20).

Here we develop a general approach for studying yet uncharacterized nucleic acid duplex defects, starting with physiologically important 8oxoG lesion, by unzipping the DNA hairpins with optical tweezers. The optical tweezers unzipping method can measure the changes in the free energy of the duplex due to lesion directly, avoiding the issues associated with the thermal melting of the 8oxoG-C containing duplexes, for which compensating enthalpy and entropy changes minimize observed changes in T_m even when changes in free energy are significant. In contrast, the hairpin elongation upon each base pair opening is unaffected by base modifications, such that the measured changes in the unzipping force are directly related to the duplex destabilization by the lesion or other modification. Thus, these experiments can directly measure the hairpin free energy for two- or three-state unfolding, enabling the individual destabilization to be recovered. To contextualize the magnitudes of the effect of the 8oxoG-C pair on duplex opening parameters, we compare it systematically to five base pair combinations that share some properties but not others in terms of size, shape and hydrogen bonding arrangement: G-C mimics the 8oxoG-C pair most closely in shape, stacking and hydrogen bonding pattern; A-T makes fewer hydrogen bonds but forms a stable canonical pair with strong base stacking; G-T makes a similar non-canonical pair by forming hydrogen bonds and matching the width of the base stack well; C-T forms an unstable base pair with weak hydrogen bonding and diminished base stacking; and 8oxoG-A contains the 8oxoG lesion but in a flipped conformation with Hoogsteen hydrogen bonding. Our results show that oxidization weakens the G-C pair, such that the lesion resembles a wobble, though destabilization is not consistent with a full mismatch. We also find surprisingly that oxidation does not diminish the stability of a G-A mismatch, in contrast to the results of some earlier studies (9,10), but in agreement with other recent measurements (21).

MATERIALS AND METHODS

Hairpin constructs

Synthesis of hairpin constructs begins with PCR amplification of pBR322 plasmid to create two ∼3 kb-long handles that are subsequently ligated to either end of the hairpin. The resulting 6.6 kb hairpin construct has a biotin and digoxigenin on opposite 5′ termini. Detailed assembly scheme and sequences are shown in Supplementary Methods S1 and is also summarized in Supplementary Figure S2.

Sequences of the DNA fragments used to create these constructs are shown in Supplementary Tables S1 and 2.

Optical tweezers and force ramp experiments

Individual hairpin constructs were isolated and tethered as shown in Figure 1 and described previously (22,23). Briefly, solutions of the hairpin construct were diluted into the experimental buffer of 10 mM HEPES (pH 7.0), and [Na$^+$] of 100 mM. A 2.1 μm diameter polystyrene bead (*Spherotech*), coated in anti-dig is fixed onto a glass micropipette (*WPI*), glued into a custom flow cell. Streptavidin-coated polystyrene beads of 5.0 and 3.0 μm diameter (*Bangs Labs*, *Spherotech*) were held in a dual-beam counter propagating optical trap (*Lumics*, *Nikon*, *Thorlabs*) (the 5.0 μm bead is shown in the figure). The flow cell is moved at a fixed loading rate of 10 pN/s, in ∼4 nm steps (*nPoint*), and increasing DNA tension is recorded by a lateral effect detector (*SpotOn*, *Melles Griot*). Though this instrument is capable of varying loading rates, faster rates compromise the signal-to-noise, while slower rates reveal drift in the micropipette position. Instrument calibration is affected by overstretching phage-λ DNA and the finite trap stiffness is measured for the beads used. Hairpin unfolding was identified and characterized as described previously (22).

Estimates of the free energy landscape using mfold

Hairpin sequences were entered into the DNA form of the mfold web server, with [Na$^+$] of 100 mM and at 22°C, to best match experimental conditions (24). mfold returned individual base energies that included base pairing and nearest neighbor (stacking) interactions. These energies were summed, starting from the base of the hairpin to give the energy required to unfold the hairpin up to a given length. While mfold includes energies of mismatched pairs of undamaged bases, it does not include the energies of oxidized bases. Initially, any 8oxoG bases were simply treated as undamaged guanines, so that the contribution to the energy sum by 8oxoG-C is identical to a canonical G-C, and that of the 8oxoG-A is identical to a mismatch G-A. When experiments revealed differences between these estimates and the data, the energy of these base pairs was changed to achieve a match with the available landscape data as discussed below.

RESULTS

Hairpin stability directly measured in unfolding experiments

The DNA hairpins in this study were unfolded/folded in an optical tweezers instrument, as discussed in the 'Materials and Methods' section and shown in Figure 1A. Hairpin sequences were based on the RNA hairpin of the transactivation response element (TAR) of the HIV-1 virion. Previous studies have shown that base pair mismatches in the lower stem lead to destabilization of the overall RNA hairpin (22). Two stable control DNA hairpins were created that feature G-C and A-T pairs at the lower part of the stem to replace these mismatches as shown in Figure 1B. Another pair of hairpins was created, replacing the canonical base pairs with two G-T mismatches and two C-T mismatches,

effectively reintroducing the base stem instabilities (compare the highlighted regions in Figure 1B). Finally, a pair of '8oxo' hairpins was created by incorporating oxidized guanine: one hairpin features two 8oxoG-C pairs and another two 8oxoG-A pairs. Base pairing under the influence of oxidative damage to guanine is contrasted to canonical pairs and mismatches in Supplementary Figure S1, while the key substitution of 8oxoG-C for G-C is shown inset to Figure 1C and D. Hairpins were created as discussed in 'Materials and Methods' section and additional details are shown in Supplementary Methods 1 while a schematic of hairpin construction may be found in Supplementary Figure S2.

Force ramp experiments isolate single hairpins and subject them to fast cycles of extension and release. Figure 1C shows several such cycles for fully matched G-C containing hairpins while Figure 1D shows cycles for hairpins substituting two 8oxoG-C base pairs in the stem according to Figure 1B. For each cycle, the gradual change in the elasticity of the double-stranded DNA (dsDNA) handles under force is evident and is fit to a polymer elasticity model detailed in Supplementary Methods 2. At a critical force, a sudden change in the length is measured and this event is identified as DNA hairpin unfolding. The length change is associated with the hairpin opening length (Δx_{op}) and both an unfolding or opening force (F_{op}) and closing force (F_{cl}) are recognized. The single-stranded DNA (ssDNA) hairpin and the dsDNA handles are also modeled as described in Supplementary Methods 2. The work of unfolding and refolding during a given cycle is the area between these two models ($W = \Delta G_{ds} - \Delta G_{ds+ss}$). The results from *n* cycles for each hairpin are discussed below.

Models of hairpin unfolding predict stem instability

mfold is frequently used to test the configuration and folding free energy of various sequences of ssDNA and ssRNA (24). The sequences of the hairpins shown in Figure 1B were submitted to the mfold server as described in the 'Materials and Methods' section. mfold returns an array of energies (including nearest-neighbor contributions), $G_i(n_i, F = 0)$ for each base pair (n_i), in the absence of any external force (F). An unfolding landscape is created by summing these energies from the stem (where unfolding must begin) to the apical loop to recover the total folding/unfolding energy; $\Sigma_i G_i(n_i, 0) = \Delta G_o$. Figure 2A shows these sums for the fully matched hairpins containing G-C and A-T base pairs at the key sites. This landscape provides theoretical estimates of the hairpin unfolding energy (ΔG_o), hairpin length (Δx_{op}) and the transition state barrier height ($\Delta G_{op}^{\dagger}$) and distance ($\Delta x_{op}^{\dagger}$), as well as an estimate of the mean unfolding force ($F_{1/2}$), all of which we will compare with experimentally determined landscape parameters below.

Increasing the tension reduces the overall stability of the hairpin, altering the energy landscape at each base pair; $G_i(n_i, F) = G_i(n_i, 0) - F\Delta x_i \cdot n_i$. The likelihood of observing hairpin unfolding increases with force, and the probability of observing the hairpin partially unfolded may be plotted ($p \sim e^{-Gi(ni, F)}$). As the force is increased further (but held constant across the hairpin extension), the total probability of observing the folded state (p_{cl}) decreases while the un-
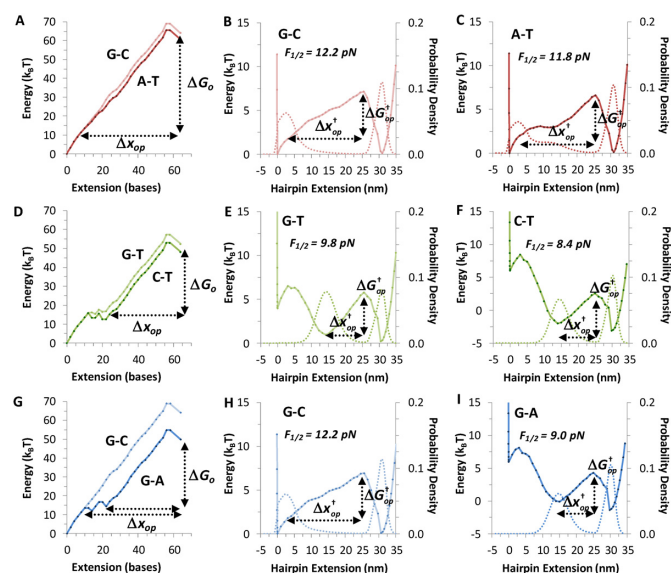
Figure 2. Predicting hairpin thermodynamics. (**A**) Summing base pair and stacking energies determined by mfold for the fully matched G-C (pink) and A-T (red) DNA hairpin sequences (shown in Figure 1B). Fully unzipping the hairpin requires a total free energy (ΔG_o), over the total hairpin length (Δx_{op}), minus a small length that frays at low force. The 'dip' near the end for all unzipping free energy profiles at zero force correspond to the unfavorable free energy associated with the hairpin loop closure. (**B**) Increasing force on the G-C hairpin will lower the free energy (solid line) of the unfolded state until the folded and unfolded states are at equal energy, at a fixed force of $F_{1/2} = 12.2$ pN for the G-C hairpin shown here. The occupancy (dotted line) is 50:50 for the folded and unfolded state. A transition barrier height ($\Delta G_{op}^\dagger$) and distance from the folded state ($\Delta x_{op}^\dagger$) may be identified. (**C**) The landscape for A-T containing hairpins at $F_{1/2}$ shows some additional fraying. (**D**) Summing base pair and stacking energies determined by mfold for the mismatch containing G-T (sage) and C-T (green) DNA hairpin sequences. Landscapes for G-T containing (**E**) and C-T containing (**F**) hairpins at $F_{1/2}$ are significantly destabilized, fraying the lowest ∼12 bp. The landscape now shows opening and closing between a stem-frayed state and the fully unfolded state at equal energy. An offset of 6 k_BT places the landscape in the same energy range as (**B** and **C**) but does not change the shape of the probability distribution. (**G**) The total energy for the 8oxoG-C (cyan) and 8oxoG-A (blue) containing hairpins are modeled in mfold with canonical guanines. The resulting landscape at $F_{1/2}$ is identical to the G-C containing hairpin (**H**) and shows little hairpin fraying, while the mismatch G-A shows significant fraying (**I**) and is offset by 6 k_BT as above. All values are summarized in Table 1. Folded and unfolded landscape potentials are added as described in Supplementary Methods S3.

folded state increases (p_{op}). At a critical force the probability of observing the folded and unfolded state is equal, $p_{op} = p_{cl}$, and this defines $F_{1/2}$. Figure 2B and C show these landscapes $G_i(x_i, F_{\frac{1}{2}})$ for G-C and A-T containing hairpins, with additional calculations available in Supplementary Methods 3. These landscapes reveal a rough transition barrier and the height of this barrier and the distance from the folded state may be identified. As expected, $F_{1/2}$ decreases with hairpin stability. However, at $F_{1/2}$ the fully folded state has a definite probability associated with a few of the lowest stem bases unfolded. This suggests that the first bases in the stem may 'fray' at low forces below $F_{1/2}$, and this fraying may be variable in length, an effect that has been seen before (22). Theoretical estimates of the hairpin unfolding

energy (ΔG_o), length (Δx_{op}) and transition state properties that account for this effect are shown in Table 1.

Replacing the matched bases with the G-T and C-T mismatches in Figure 2D further reduces the overall hairpin energy and the critical unfolding force ($F_{1/2}$). Importantly, in these mismatched cases the entire lower stem is destabilized relative to the upper part of the hairpin. Instead of a two-state transition from a folded to an unfolded state, unfolding is observed to proceed through an intermediate, partially unfolded state. The lowest 10–14 bp unfold at a low force (<8 pN), a small length change that is not typically resolved in these experiments. The upper stem unfolding, occurring at high force (where the signal to noise is greater) is characterized in these experiments. The unfolding landscape is adjusted until the probability of observing the intermediate state and the unfolded state is equal. This is most accurately done with the lowest stem removed, though this result is superimposed upon the full landscapes (with a vertical offset) in Figure 2E and F for comparison to the matched hairpins. Thus, the presence of these mismatches causes a dramatic and easily identified change in every landscape parameter.

Hairpin unfolding energies reveal oxidative damage

Energies of base pairs containing the oxidized guanines, 8oxoG-C and 8oxoG-A, have not been thoroughly characterized by thermal melting and thus are not specifically included in the mfold database. To approximate the landscape, we assumed initially that these base pairs are identical to their undamaged counterparts G-C and G-A, as shown in Figure 2G–I. Though by this model a hairpin containing 8oxoG-C appears fully stable, the mismatch 8oxoG-A shows a significant reduction in measured length and an energy associated with an intermediate state as shown above. Estimated parameters are collected in Table 1, where they will be compared to measurements described below.

Though the measured distributions of the work of folding and unfolding (W) are not measured in equilibrium with hairpin unfolding, the equilibrium hairpin unfolding energy (ΔG_o) may be faithfully retrieved using methods developed by Crooks (25) and Bennett (26). Figure 3A and B shows the determination of unfolding free energies for the fully matched hairpins. These techniques are discussed more fully in Supplementary Methods 4, and sample distributions are shown in Supplementary Figure S3 for comparison. When the key G-C sites are replaced with A-T, the overall energy is reduced modestly. However, substitution of the mismatches G-T, C-T or 8oxoG-A clearly causes the significant reduction in unfolding energy associated with lower stem loss described above. Furthermore, this energy change is evident for 8oxoG-C as well, indicating that this base pair weakens the hairpin compared to G-C.

The landscape of the matched G-C hairpin was adapted to model the 8oxoG-C pair by removing a fixed energy of 6.0 k_BT at the two sites indicated in Figure 3C, giving rise to the landscape of Figure 3D. To match the full change in stability, both the 8oxoG-C and the nearest neighbor were weakened by this amount (four sites ware affected for a total of 12.0 k_BT for the two lesions). While it is possible that some sites were weakened differentially, distinctions between them could not be accurately judged in this work.

Table 1. Comparisons between theory and experiment for DNA hairpin unfolding

Hairpin	*n*	ΔG_o (k_BT)	Δx_{op} (bases)	$F_{1/2}$ (pN)	(k_BT) @$F_{1/2}$	(bases) @$F_{1/2}$
Control G-C	110	56.0 ± 0.4	55.8 ± 0.3	12.5 ± 0.1	7.8 ± 1.5	37 ± 2
		55 ± 1	*55 ± 1*	*12.2 ± 0.2*	*7.1 ± 1.5*	*44 ± 2*
Control A-T	57	53.6 ± 0.4	52.4 ± 0.7	11.9 ± 0.1	-	-
		52 ± 1	*54 ± 1*	*11.8 ± 0.2*	-	-
Mismatch G-T	98	36.8 ± 0.4	42.0 ± 0.6	9.7 ± 0.1	6 ± 2	23 ± 4
		36 ± 1	*38 ± 1*	*9.8 ± 0.2*	*5 ± 2*	*26 ± 4*
Mismatch C-T	55	27.6 ± 0.4	31.3 ± 0.8	7.8 ± 0.1	-	-
		28 ± 1	*30 ± 1*	*8.4 ± 0.2*	-	-
8oxoG-C	92	35.2 ± 0.4	38.7 ± 0.5	9.5 ± 0.1	5 ± 2	24 ± 4
		36 ± 1	*38 ± 1*	*9.8 ± 0.3*	*6 ± 2*	*28 ± 4*
8oxoG-A	39	32.0 ± 0.4	37.0 ± 0.9	9.4 ± 0.2	-	-
		31 ± 1	*34 ± 1*	*9.0 ± 0.3*	-	-

The number of extension/release cycles (*n*) shown for optical tweezers unfolding/folding experiments shown in Figure 1. Measurements of the hairpin unfolding free energy (ΔG_o) found from fits to Supplementary Equations S5 and S6, as shown in Figure 3. The unfolding length (Δx_{op}) is compared for these constructs in Figure 4. The force at which folding and unfolding occur at equal rates ($F_{1/2}$) found from the force unfolding distributions of Figure 5. Fits of unfolding distributions to Supplementary Equation S6 and S7 are shown in Figure 5 for three constructs, giving the transition barrier height ($\Delta G_{op}^{\dagger}$) and distance from the folded state ($\Delta x_{op}^{\dagger}$). Theoretical values found from mfold energy landscape calculations detailed in Figure 2, and shown in italics below each experimental result. The values for 8oxoG-C and 8oxoG-A were determined from landscapes for G-C and G-A. The values for 8oxoG-C required an additional destabilizing energy of 6.0 k_BT at each site, while the values for 8oxoG-A were stabilized by 0.4 k_BT, to yield a match to experimental values. Details of this iterative calculation discussed in the text.

Critically, this energy decrease causes a key change in the landscape; the 8oxoG-C containing hairpins are now predicted to show the release of the lower stem. Figure 3E and F show the change to the energy landscape of the G-A containing hairpin, and the slight total energy *increase* of 2.0 k_BT at each site required to match the observed experimental unfolding energy of 8oxoG-A. Importantly, this change does not cause any further significant change to the landscape and is even within the uncertainty of the energy measurement. Figure 3G compares all the experimental and theoretical results, showing excellent agreement for the canonical pairs and the mismatches. Furthermore, these results clearly illustrate the destabilization induced by oxidative damage to the G-C base pair not covered by mfold, while the 8oxoG-A pair is nearly identical within experimental uncertainty to the G-A. The latter result is somewhat surprising, given that the 8oxoG is flipped into the G_{syn}-A_{anti} conformation, as explained below.

The overall opening length of unfolding (Δx_{op}) was measured for each extension/release cycle, and these distributions are shown for each hairpin in Figure 4A–F. The average unfolding length was converted into a number of bases using the force-dependent elasticities discussed in Supplementary Methods 2. The results are shown in Table 1 and Figure 4G. The measured lengths of the fully matched hairpins compare well with expected values and nearly match the full hairpin lengths, as ~55 bases are observed during opening, compared to 64 bases for the known structure. The difference is due to stem fraying, as described above. The values for the mismatch and damaged base containing hairpins all show evidence of a further length reduction as only ~40 bases are released upon opening, due to the loss of the lowest part of the stem at lower forces. Crucially, in one case, that of the G-T containing hairpin, an initial event could be deduced for ~50% of the hairpins and this showed a release of 18 ± 1 bases, which compares well with the difference between the fully matched and mismatch/damage-containing hairpins. Unfortunately, these short opening events (<8 nm)

could not be reliably resolved at forces below 5 pN ($F_{1/2}$ ∼ 6 pN for the events seen in the G-T containing hairpin).

Finally, the distribution of unfolding forces $P(F_{op})$ provides insight into the transition state. The distribution for the fully matched G-C containing hairpin is shown in Figure 5A. The value of the force at the peak represents $F_{1/2}$ which is equal to the average force within uncertainty. Furthermore, this distribution may be fit to a model of force-influenced unfolding of Dudko, *et al.*, described in the Supplementary Methods 5 (27,28). These fits returned values of the barrier height ($\Delta G_{op}^{\dagger}$) and distance ($\Delta x_{op}^{\dagger}$). These values may be compared to those obtained from the unfolding force distributions for G-T and 8oxoG-C containing hairpins, shown in Figure 5B and C. Comparing the unfolding force ($F_{1/2}$) for all hairpins, as shown in Figure 5D, confirms the prediction that the unfolding force decreases for defect-containing hairpins. For the three hairpins fitted here, the full energy landscapes may be contrasted and compared to theoretical landscapes from above in Figure 5E–G. Changes in the transition state overlap predictions well, and this serves to confirm both the decrease in the unfolding free energy and loss of the lowest stem described above. Furthermore, weakened hairpins are observed to have smaller barriers, which lie closer to the folded state, as opposed to hairpins where the barrier lies relatively far from the folded state, such as seen for TAR RNA (22). The landscape for 8oxoG-C containing hairpins is fully consistent with the destabilized site model, which gives matches for all of the values of the landscape parameters in including not just the hairpin unfolding energy (ΔG_o), but the opening length of hairpin unfolding (Δx_{op}), the barrier height ($\Delta G_{op}^{\dagger}$) and distance from the folded state to the transition state ($\Delta x_{op}^{\dagger}$). Finally, the correlation of the graphs for ΔG_o, Δx_{op} and $F_{1/2}$ (Figures 3G, 4G and 5D) are correlated, as the stability and length of the of the frayed hairpins are roughly proportional. However, the transition force changes somewhat less as it is the ratio $F_{1/2} \sim \Delta G_o / \Delta x_{op}$.
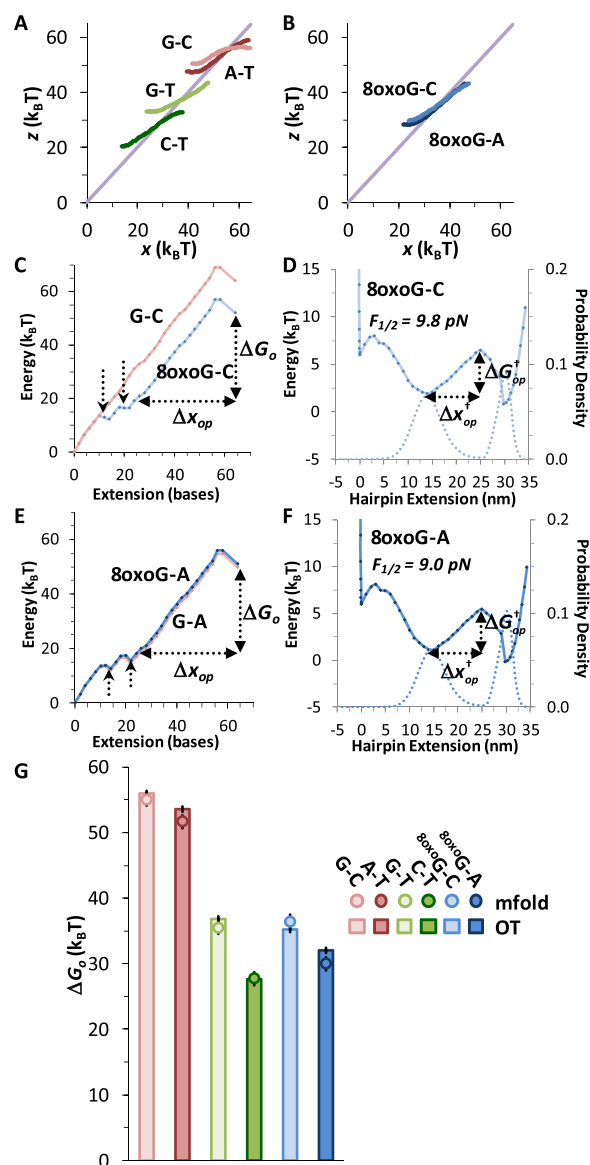
Figure 3. Hairpins are directly destabilized by stem substitutions. Measuring the unfolding hairpin energy as the crossing point of each cumulative work distribution $z(x)$ and the line $z = x$ gives the equilibrium unfolding energy (ΔG_o). This method is described more fully in Supplementary Methods S4 ([26],[29]). (**A**) The crossing point for the fully matched G-C (pink) and A-T (red) hairpins as well at the mismatch containing G-T (sage) and C-T (green). (**B**) Measurement of the equilibrium free energy of the 8oxoG-C (cyan) and 8oxoG-A (blue) containing hairpins. (**C** and **D**) Hairpin free energy profile for G-C containing hairpins (pink). To match the measured free energy of the 8oxoG-C substituted hairpins, the two sites shown by the arrows were each destabilized by 6.0 k_BT. This free energy profile (blue) leads to a landscape that shows significant fraying, as opposed to the value predicted from mfold for G-C. (**E** and **F**) Hairpin free energy profile for G-A containing hairpins (pink). To match the measured free energy of the 8oxoG-A substituted hairpins, the two sites shown by the arrows were each *stabilized* by 0.4 k_BT. This free energy profile (blue) leads to a landscape that that is effectively the same within uncertainty compared to the G-A landscape of Figure 2. (**G**) Comparisons of the predicted and measured hairpin free energy. Measured lengths from OT experiments shown as vertical bars, while values predicted from mfold (Figure 2) are shown as circles. Introducing mismatched and damaged bases increases stem fraying and leaves a weaker hairpin, compared to the G-C containing hairpin. Values are also summarized in Table 1. All errors represent the standard error in the mean.

Individual base instabilities

While it is instructive to study the stability of a full or partial hairpin, it is important to consider the average stability of these two key sites for each substitution. The base pair energies from mfold may be easily compared along the full landscape, using Figure 2A as a starting point and taking the matched hairpin containing G-C pairs at the key sites as a reference. The only difference occurs at four sites—the substituted bases and the nearest neighbors, and we average those differences. The individual G-C energy is found directly from mfold or calculated from the underlying data and consists of the energy predicted by mfold at each site, including the nearest neighbor energy ([24]). Each substitution is directly compared to this number to give the theoretical stability per site. Alternatively, there are the landscapes of each hairpin (of Figure 2A and D), subtracted from the G-C landscape and expressed per site. For 8oxoG-C and 8oxoG-A, the difference is simply the increase or decrease that was modeled at each site to match the change in the hairpin energy. Experimental values are found from the optical tweezers data, adding back the energy of the frayed stem, then comparing the overall energies relative to G-C, as above. The results are shown numerically in Table 2, and graphically relative to the G-C match in Figure 6. While G-C and A-T base pairs contribute to hairpin stability, the inclusion of G-T, C-T and 8oxoG-A mismatches *destabilize* the hairpin. Finally, 8oxoG-C also destabilizes the hairpin, by an amount that closely corresponds to the G-T 'wobble', but by less than the full mismatches.

DISCUSSION

Stability of canonical and mismatched base pairs in DNA

Many studies over the last two decades have illustrated the power of force-induced denaturation with optical tweezers to elucidate the folding and unfolding pathways and overall stability of biomolecules ([29–31]). Here we demonstrate that the measured unfolding forces, energies, and transition state lengths of DNA hairpins agree well with mfold models derived from thermal melting techniques, both for hairpins containing canonical bases as well as those containing mismatched G-T and C-T base pairs. This agreement supports the use of optical tweezers to extend our understanding of DNA unfolding into new, uncharacterized systems that are not currently a part of the mfold database such as 8oxoG. Indeed, the integration of the force data with mfold to map out transition state models for unfolding confirms the power of using both methods in a complementary fashion. Furthermore, the force-unfolding method may characterize the transition state and a simple energy landscape that provides additional quantitative information on the unfolding pathway.

In melting DNA hairpin duplexes by force, we show that both G-C and A-T canonical base pairs contribute favorably to the stability of the duplex (Table 2), with A-T contributing less than G-C as expected. In contrast, all other base pairing combinations tested are destabilizing. In our hairpin assemblies, G-T mismatches only modestly destabilize the DNA duplex in which they are found. An X-ray crystal structure of the G-T mismatch shows that these
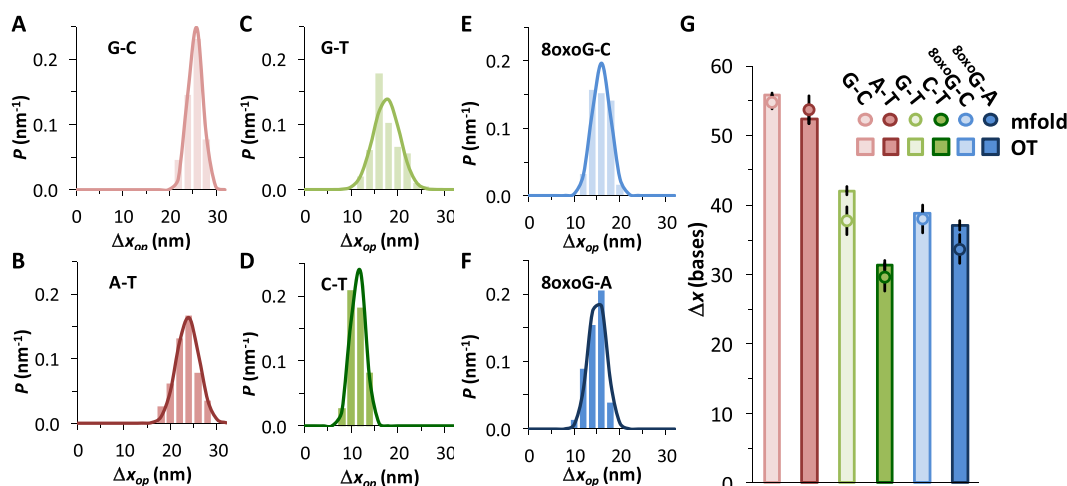
Figure 4. Mismatches greatly increase stem fraying. Distributions of the measured unfolding length (Δx_{op}) for the (**A**) fully matched hairpin including G-C at the selected sites, (**B**) fully matched hairpin with A-T substitutions, (**C**) mismatch G-T containing hairpin, (**D**) mismatch C-T containing hairpin and hairpins with (**E**) 8oxoG-C and (**F**) 8oxoG-A substituted at the key sites (Figure 1). The mean unfolding length decreases, as mismatch and oxidized base substitutions cause fraying of the lower stem that effectively reduces the folded hairpin length. (**G**) Comparisons for all hairpin substitutions in this study. Measured lengths from OT experiments are shown as bars, while values predicted from mfold landscapes of Figure 2 are shown as circles. While the A-T substitutions do not fray the stem, base pair mismatches and oxidatively damaged bases do. Results are summarized in Table 1.
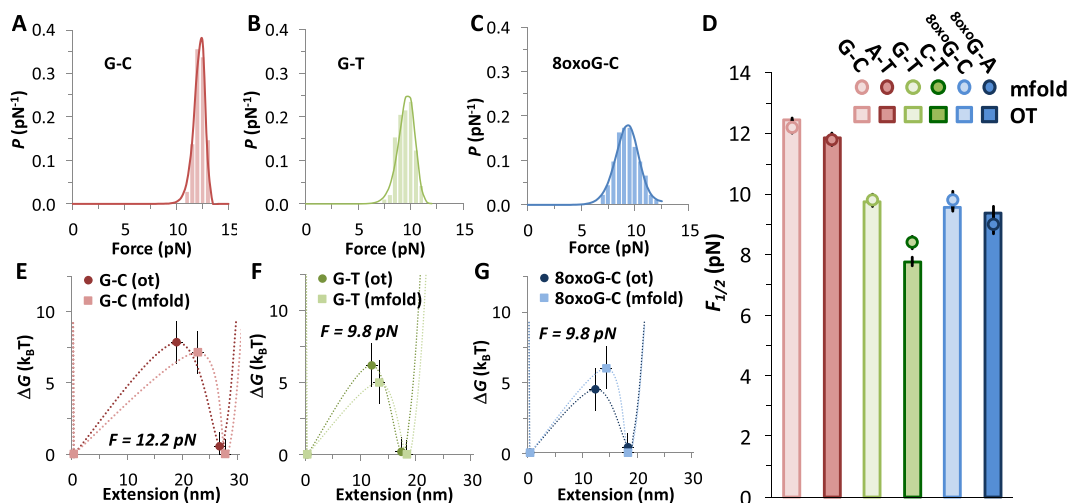

Figure 5. Unfolding forces decrease for mismatch containing hairpin stems. (**A**) The measured distribution of the unfolding force ($P(F_{op})$) for fully matched G-C containing hairpins. Data are fit to the unfolding model of Dudko (Supplementary Equations S6 and S7, solid line) as shown in Supplementary Methods S5. (**B**) Unfolding force distribution ($P(F_{op})$) for G-T containing hairpins and fit (solid line). (**C**) Unfolding force distribution ($P(F_{op})$) and fit (solid line) for damaged 8oxoG-C containing hairpins, where the peak unfolding force is reduced by stem fraying. Fitted values of the barrier height ($\Delta G_{op}^{\dagger}$) and distance ($\Delta x_{op}^{\dagger}$) are reported in Table 1. (**D**) The force at which hairpin folding and unfolding are equally probable ($F_{1/2}$), plotted for the hairpins in this study. OT data shown in bars while theoretical predictions are plotted as circles. Weakened hairpins unfold at lower forces, and values are also summarized in Table 1. (**E**) Unfolding landscape composed of values of the unfolding free energy (ΔG_o), the unfolding length (Δx_{op}), the barrier height ($\Delta G_{op}^{\dagger}$) and distance ($\Delta x_{op}^{\dagger}$) for fully matched, G-C containing hairpins. Theory (pink squares) and experiment (red circles) compare well at the peak unfolding force ($F_{1/2}$), where the folded and unfolded states have equal energy. (**F**) Landscape for G-T containing hairpins. Theory (sage squares) and experiment (green circles) are compared at the peak unfolding force ($F_{1/2}$). (**G**) Landscape for 8oxoG-C hairpins. Theoretical landscape parameters (cyan squares) are plotted alongside experimentally measured values (blue circles). Values of the hairpin energy (ΔG_o), opening length (Δx_{op}) and barrier energy ($\Delta G_{op}^{\dagger}$) and distance ($\Delta x_{op}^{\dagger}$) for all of the fits are all summarized in Table 1.

Table 2. Base pair stability reduced by oxidative damage

Base Pair	ΔG_o (k_BT) *mfold*	ΔG_o (k_BT) OT	ΔG_o (kcal/mol) *mfold*	ΔG_o (kcal/mol) OT
G-C	5.2 ± 0.2	5.2 ± 0.2	8.8 ± 0.3	8.8 ± 0.3
A-T	3.5 ± 0.2	3.7 ± 0.2	5.9 ± 0.3	6.2 ± 0.3
G-T	-0.6 ± 0.2	-0.6 ± 0.4	-1.1 ± 0.3	-1.0 ± 0.7
C-T	-2.8 ± 0.2	-3.0 ± 0.4	-4.7 ± 0.3	-5.1 ± 0.7
8oxoG-C	-1.2 ± 0.2	-1.2 ± 0.4	-2.0 ± 0.3	-2.0 ± 0.7
8oxoG-A	-1.9 ± 0.2	-2.1 ± 0.4	-3.2 ± 0.3	-3.5 ± 0.7

Individual base pair energy contribution to hairpin stability (in k_BT and kcal/mol), also shown in Figure 6. Because DNA damage affects the base and its nearest neighbor, the stability for G-C and A-T base pairs includes the free energy of the nearest neighbor. Experimental values found from optical tweezers unfolding experiments, including removal of the estimation of the lower stem energy as described in the text. Theoretical values found directly from mfold, though for 8oxoG-C the stability of the oxidized guanine and its nearest neighbor were reduced by 6.0 k_BT (10 kcal/mol), and for 8oxoG-A the stability of the oxidized guanine and its nearest neighbor were increased by 0.4 k_BT (0.7 kcal/mol) to match observed experimental results.
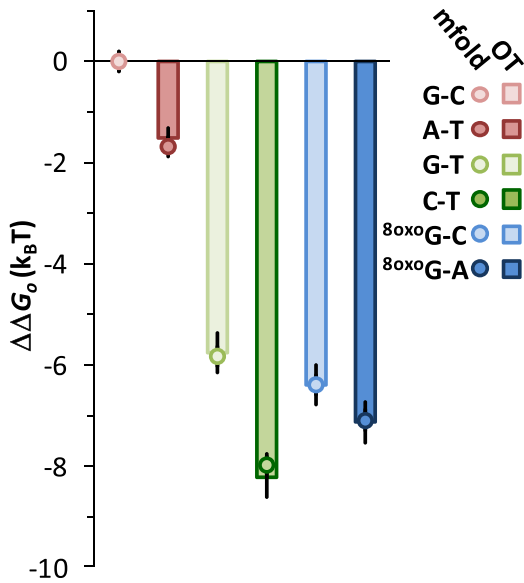

Figure 6. Oxidative damage disrupts base stacking. Average base pair energy of the substituted sites (shown in yellow in Figure 1B), relative to the stability of a G-C containing pair. Values from mfold (circles) are compared to measured values (bars) as determined from unfolding experiments discussed in the text. Relative to either G-C and A-T pairs, the presence of G-T and C-T mismatches will destabilize a hairpin. Oxidative damage also destabilizes the hairpin, as 8oxoG-C is 6.4 k_BT less stable than G-C, with a stability that resembles the G-T wobble. However, the destabilization of 8oxoG-A matches the destabilization predicted for G-A, as discussed in the text.

bases pair in the helix by forming two hydrogen bonds in a 'wobble' pairing motif (32). Nuclear magnetic resonance (NMR) spectra from previous work show sharp peaks for the G and T imino protons as well as flanking base pairs, confirming that hydrogen bonding is robust (33), though the base pair opening rate is ~300× faster for G-T than G-C (34). The C-T mismatch is the most destabilizing to the double helical form of DNA studied in this work. NMR data show that the H-bonding is weak, supporting models in which the C-T pair forms longer or water-mediated H-bonds (35). The imino proton on T is present but lacks NOE cross-peaks due to fast exchange with water, consistent with more recent MD simulations that predict two non-canonical base pairing conformations of similar energies (36).

Oxidative damage induces destabilization

The ΔG_o of the 8oxoG-C base pair is negative, meaning that the presence of the 8oxoG-C pair actively *subtracts* from the stability of the DNA duplex in which it is found (Table 2). When compared to the relative thermodynamic contributions of *all* undamaged base pairs in all sequence contexts as determined by Poyret *et al.* (37), it is clear that 8oxoG-C behaves like mismatched bases rather than a matched pair. Our results directly quantify the energy loss during the substitution of 8oxoG-C for G-C to be -6.0 ± 0.4 k_BT, including both the destabilization of base pairing and disruption of the nearest neighbor upon which this value also depends (38). This concrete value for 8oxoG-C destabilization may be useful to other workers who are modeling recognition and binding by hOGG1 and MutM.

The thermodynamic destabilization induced by the 8oxoG-C base pair is notable because it stacks normally on its neighbors and forms three hydrogen bonds. Previous NMR analysis has shown that the imino proton exchange time with solution is indistinguishable for G-C versus 8oxoG-C pairs (14,15). The latter study also showed that the natural rates of base pair opening and closing, k_{op} and k_{cl}, are not very different for the G-C and 8oxoG-C pairs. Nonetheless, the NMR method may overlook small changes in stability, since imino proton exchange may not detect all states with altered pairing and stacking.

Though most similar to a G-C pair structurally, *thermodynamically* the 8oxoG-C pair is most similar to the G-T 'wobble' pair, in which guanine also forms hydrogen bonds to a pyrimidine neighbor and stacks within the helix, though with a shear (32). Provocatively, quantum mechanical calculations indicate that the addition of the carbonyl oxygen at C8 and a proton at N7 to guanine (forming 8-oxoG) causes a rotation of the base dipole by 42° (39), which would be expected to alter the electrostatic contribution to 8oxoG base stacking on its nearest neighbors despite the similarity in buried surface area, but in a way that is difficult to calculate precisely (40). Though sugar pucker at the 8oxoG-C pair appears to fall into the normal C2′*endo* range (4), phosphorus NMR data hint that the backbone may switch from the normal BI to BII conformation adjacent to the lesion, with a corresponding reduction in twist (41). Though DNA melting experiments show only a small change in the measured melting temperature of 8oxoG-containing duplexes relative to the corresponding G-containing duplexes, the derived free energy change for

melting is more significant, in agreement with the findings of this work (10,38). A combination of calorimetric methods showed that this effect is associated with a slight reduction of the number of counterions and significant reduction of ∼15 water molecules upon substitution of 8oxoG-C for G-C (41). The 8oxoG-C duplex appears much less hydrated than the G-C duplex, due to additional O and H of the O8 and N7 atoms in the major groove. In both cases the duplex form of DNA is more hydrated than ssDNA, but less so for 8oxoG-C.

The 8oxoG-A pair is unique because it has attributes of both an oxidized base and weakened base pairing. Importantly, 8oxoG-A is conformationally dissimilar to the G-A pair, as 8oxoG is flipped into the *syn* orientation and hydrogen bonds with adenine via its Hoogsteen edge instead of the Watson–Crick edge. Our optical tweezers results reveal that substitution of 8oxoG-A contributes an energy loss of $7.3 \pm 0.4\,k_BT$ to the hairpin at each site (compared to the G-C control), making it more unstable than an 8oxoG-C pair but less unstable than the C-T mismatch. This number is ∼2 k_BT per site greater than previously found in spectroscopic and thermodynamic measurements, though salt concentrations and sequence context differ (10). Interestingly, Plum *et al.* observed that the substitution of 8oxoG-A pair was less destabilizing than the G-A pair (but more than 8oxoG-C), a result that was explained by the *syn-anti* conformational differences in the guanine glycosidic bond angle. In our system, the measured destabilization of the 8oxoG-A pair is directly comparable within uncertainty to the mfold calculated energy of the G-A mismatch; no additional corrections need be added to the mfold model to account for the oxidative lesion. Nonetheless, both results show that the negative thermodynamic effect of the 8oxoG is not additive with the G-A mismatch, likely because the additional carbonyl oxygen and imine nitrogen groups on the 8oxoG provide new hydrogen bonding partners that stabilize the G_{syn}-A_{anti} conformation relative to other non-canonical conformations favored by the G-A pair (12,42). Either result (of equal energy or even decreased energy) could contribute to the ability of 8oxoG-A to avoid enzymatic repair, and lead to the G→T transversion mutation (10).

One consequence of this local instability is the reduced unfolding lengths of the hairpins containing 8oxoG or mismatches. The control hairpins with canonical matched bases open cooperatively in one unzipping event of 52–56 bases, and can be described cleanly with a two-state model. The presence of two destabilizing base pairs in the hairpin leads to fraying of the stem at very low forces, to the extent that the opening of the first part of the stem cannot be measured. In the context of genomic DNA, this implies that 8oxoG or other damaged bases could create flaws or kinks that break up the DNA helix into smaller, non-cooperative domains that are easier to open. In other recent work the effect of 8oxoG-C and several other more severe G modifications were also studied by dsDNA unzipping via pulling of the ds/ss DNA hybrid through the hemolysin pore (21,43). This approach characterized the relative kinetics of G-C unzipping. While canonical and weakly destabilizing duplex modifications led to cooperative dsDNA melting in a single step, more severe duplex defects revealed two-step dsDNA melting, mirroring the work of this paper.

While pore translocation experiments did not directly measure base pair energies, the measured rates indicated that relative to G-C, 8oxoG-C pairs were less stable and both G-A and 8oxoG-A were even less so. Notably, consistent with this work no measurable difference was seen between the G-A mismatch and the oxidized 8oxoG-A (21).

DNA-binding enzymes respond to the weaker duplex

Though the changes introduced by 8oxoG-C pairs are subtle, they have a significant effect on EcoRI enzyme activity on DNA (41). Even when 8oxoG is located at the edge of the 5′-GAATTC-3′ recognition site and not adjacent to the site of cleavage, binding and cleavage by this restriction enzyme is negatively affected by 8oxoG-C base pairs (K_M increases and k_{cat} decreases). But if the rate of base pair opening is essentially unaffected, how could a repair enzyme recognize a damage site? Recent simulations together with NMR structural studies of these duplexes that include the effect of water and counterions suggest that the restriction enzyme EcoRI probably recognizes defective duplex base pairs by a combination of local duplex unwinding, changes in the backbone conformation, and very different local hydration patterns (41). These are enough to prevent the cleavage activity of EcoRI and other restriction enzymes. We hypothesize that these phenomena may also lead to a *longer* time that excision repair proteins like MutM spend at locations containing 8oxoG. Thus, while the opening time for the 8oxoG-C pair may not be faster, the time that MutM spends on that defective base pair duplex may be longer and sufficient for that base pair to spontaneously open to be trapped and excised.

For base excision glycosylases, recognition of the 8oxoG lesion in the context of the DNA duplex occurs prior to base extrusion into the protein active site (20). Though the 8oxoG-C-associated duplex deformation in the absence of protein binding appears negligible (36), the repair glycosylases distort lesion-containing DNA significantly, supporting the proposal that the 8oxoG-C base recognition depends on higher local duplex deformability during interrogation by the editing enzyme (16). Indeed, recent modeling work (44) has found that in complex with OGG1 or MutM glycosylases the 8oxoG-C pair starts extruding from the duplex due to bending induced by partial intercalation or 'verging' of the protein aromatic residue (Tyr203 for OGG1) from the minor groove side. According to this modeling study, 8oxoG-C base pair opening only costs 1−2 kcal/mol (1.7–2.7 k_BT), compared to the cost of base pair opening in the context of un-deformed B-DNA duplex of ∼10 kcal/mol (17 k_BT). Easier 'verging' of the aromatic residue of the editing enzyme in turn likely derives from duplex destabilization induced by that lesion, which according to this and other works is moderate but significant (∼5.2 k_BT or 3.1 kcal/mol). This 'verging' is probably facilitated by easier 8oxoG-C containing duplex DNA bending into the major groove due to its much weaker hydration in combination with the weaker stacking due to the altered base 8oxoG-C dipole. All of these processes occur on the time scale of 1 s in fast pre-equilibrium with the subsequent much slower steps of enzyme conformational change and base excision, which occur over longer time scales (∼50 s).

In conclusion, in this work we attempted for the first time to use the DNA hairpin unzipping approach to characterize the effect of G→8oxoG modification on DNA duplex stability. We showed that we can quantitatively describe the effect on DNA hairpin stability of changes of DNA stem composition, including base mismatches. In this case the observed changes in the hairpin unzipping free energy profile quantitatively matched mfold predictions. However, the effect of lesions such as 8oxo-G on DNA stability cannot be predicted directly by mfold. By adapting the mfold-calculated landscape to account for the presence of lesions, we find that oxidative damage strongly destabilizes the G-C base pair. As base pairing is not affected by 8oxoG modification of the G-C pair, it is changes in stacking that are responsible for local duplex destabilization, comparable in magnitude to that introduced by mismatches. This result agrees with the finding of Yakovchuk *et al.* that base stacking interactions largely determine duplex stability (45). We also find that oxidative damage does not affect the energy of the G-A mismatch, in contrast to previous thermodynamic measurements obtained under different solution conditions (10), but in agreement with more recent nanopore stability measurements (21). Together, our results suggest that while base pair opening and closing may not be strongly affected by the 8oxoG modification, hydration and overall base pair stability are strongly affected, and this could provide a mechanism for repair enzyme recognition. This localized destabilization leads to a less stable hairpin (Figure 3) that unfolds at lower forces (Figure 5). In the cell, the opening of the DNA duplex into other conformations such as replication forks, transcription bubbles and base-extruded repair states is achieved not by increasing temperature but by the action of a variety of different enzymes that exert forces on the DNA during their function. Furthermore, the DNA experiences significant stresses due to supercoiling, packaging into chromatin and binding of regulatory proteins that bend and stretch the DNA. These stresses would be expected to highlight 8oxoG-containing defects in the DNA such as those measured here.

SUPPLEMENTARY DATA

Supplementary Data are available at NAR Online.

ACKNOWLEDGEMENTS

FUNDING

REFERENCES

1. Burrows,C.J. and Muller,J.G. (1998) Oxidative nucleobase modifications leading to strand scission. *Chem. Rev.*, **98**, 1109–1151.
2. Dedon,P.C. (2011), Oxidation and Deamination of DNA by Endogenous Sources. In: Penning,TM (ed). *Chemical Carcinogenesis*. Humana Press, NY, pp. 209–225.
3. Friedberg,E.C., Walker,G.C., Siede,W., Wood,R.D., Schultz,R.A. and Ellenberger,T. (2006) *DNA Repair and Mutagenesis*. 2nd edn. ASM Press, Washington, DC.
4. Bowman,B.R., Lee,S., Wang,S. and Verdine,G.L. (2008) Structure of the *E. coli* DNA glycosylase AlkA bound to the ends of duplex DNA: A system for the structure determination of lesion-containing DNA. *Structure*, **16**, 1166–1174.
5. Lipscomb,L.A., Peek,M.E., Morningstar,M.L., Verghis,S.M., Miller,E.M., Rich,A., Essigmann,J. and Williams,L.D. (1995) X-ray structure of a DNA decamer containing 7,8-dihydro-8-oxoguanine. *Proc. Natl. Acad. Sci. U.S.A.*, **92**, 719–723.
6. Hsu,G.W., Ober,M., Carell,T. and Beese,L.S. (2004) Error-prone replication of oxidatively damaged DNA by a high-fidelity DNA polymerase. *Nature*, **431**, 217–221.
7. Shibutani,S., Takeshita,M. and Grollman,A.P. (1991) Insertion of specfic bases during DNA synthesis past the oxidation-damaged base 8-oxodG. *Nature*, **349**, 431–434.
8. McAuley-Hecht,K.E., Leonard,G.A., Gibson,N.J., Thomson,J.B., Watson,W.P., Hunter,W.N. and Brown,T. (1994) Crystal structure of a DNA duplex containing 8-hydroxydeoxyguanine-adenine base pairs. *Biochemistry*, **33**, 10266–10270.
9. Kornyushyna,O., Berges,A.M., Muller,J.G. and Burrows,C.J. (2002) In vitro nucleotide misinsertion opposite the oxidized guanosine lesions spiroiminodihydantoin and guanidinohydantoin and DNA synthesis past the lesions using Escherichia coli DNA polymerase I (Klenow fragment). *Biochemistry*, **41**, 15304–15314.
10. Plum,G.E., Grollman,A.P., Johnson,F. and Breslauer,K.J. (1995) Influence of the oxidatively damaged adduct 8-oxodeoxyguanosine on the conformation, energetics, and thermodynamic stability of a DNA duplex. *Biochemistry*, **34**, 16148–16160.
11. Collins,A.R., Cadet,J., Moller,L., Poulsen,H.E. and Vina,J. (2004) Are we sure we know how to measure 8-oxo-7,8-dihydroguanine in DNA from human cells? *Arch. Biochem. Biophys.*, **423**, 57–65.
12. David,S.S., O'Shea,V.L. and Kundu,S. (2007) Base-excision repair of oxidative DNA damage. *Nature*, **447**, 941–950.
13. Fromme,J.C., Banerjee,A., Huang,S.J. and Verdine,G.L. (2004) Structural basis for removal of adenine mispaired with 8-oxoguanine by MutY adenine DNA glycosylase. *Nature*, **427**, 652–656.
14. Crenshaw,C.M., Wade,J.E., Arthanari,H., Frueh,D., Lane,B.F. and Núñez,M.E. (2011) Hidden in plain sight: subtle effects of the 8-oxoguanine lesion on the structure, dynamics, and thermodynamics of a 15-base pair oligodeoxynucleotide duplex. *Biochemistry*, **50**, 8463–8477.
15. Every,A.E. and Russu,I.M. (2013) Opening dynamics of 8-oxoguanine in DNA. *J. Mol. Recognit.*, **26**, 175–180.
16. Bruner,S.D., Norman,D.P.G. and Verdine,G.L. (2000) Structural basis for recognition and repair of the endogenous mutagen 8-oxoguanine in DNA. *Nature*, **403**, 859–866.
17. Chen,L., Haushalter,K.A., Lieber,C.M. and Verdine,G.L. (2002) Direct visualization of a DNA glycosylase searching for damage. *Chem. Biol.*, **9**, 345–350.
18. Fromme,J.C. and Verdine,G.L. (2002) Structural insights into lesion recognition and repair by the bacterial 8-oxoguanine DNA glycosylase MutM. *Nat. Struct. Biol.*, **9**, 544–552.
19. Li,H., Endutkin,A.V., Bergonzo,C., Fu,L., Grollman,A., Zharkov,D.O. and Simmerling,C. (2017) DNA deformation-coupled recognition of 8-oxoguanine: conformational kinetic gating in human DNA glycosylase. *J. Am. Chem. Soc.*, **139**, 2682–2692.
20. Qi,Y., Spong,M.C., Nam,K., Banerjee,A., Jiralerspong,S., Karplus,M. and Verdine,G.L. (2009) Encounter and extrusion of an intrahelical lesion by a DNA repair enzyme. *Nature*, **462**, 762–766.
21. Schibel,A.E.P., Fleming,A.M., Jin,Q., An,N., Liu,J., Blakemore,C.P., White,H.S. and Burrows,C.J. (2011) Sequence-specific single-molecule analysis of 8-Oxo-7,8-dihydroguanine lesions in DNA based on unzipping kinetics of complementary probes in ion channel recordings. *J. Am. Chem. Soc.*, **133**, 14778–14784.

22. McCauley,M.J., Rouzina,I., Manthei,K.A., Gorelick,R.J., Musier-Forsyth,K. and Williams,M.C. (2015) Targeted binding of nucleocapsid protein transforms the folding landscape of HIV-1 TAR RNA. *Proc. Natl. Acad. Sci. U.S.A.*, **112**, 13555–13560.

23. Chaurasiya,K.R., Paramanathan,T., McCauley,M.J. and Williams,M.C. (2010) Biophysical characterization of DNA binding from single molecule force measurements. *Phys. Life Rev.*, **7**, 299–341.

24. Zuker,M. (2003) Mfold web server for nucleic acid folding and hybridization prediction. *Nucleic Acids Res.*, **31**, 3406–3415.

25. Crooks,G.E. (1999) Entropy production fluctuation theorem and the nonequilibrium work relation for free energy differences. *Phys. Rev. E*, **60**, 2721–2726.

26. Bennett,C.H. (1976) Efficient estimation of free energy differences from Monte Carlo data. *J. Comput. Phys.*, **22**, 245–268.

27. Dudko,O.K., Hummer,G. and Szabo,A. (2006) Intrinsic rates and activation free energies from single-molecule pulling experiments. *Phys. Rev. Lett.*, **96**, 108101–108104.

28. Dudko,O.K., Hummer,G. and Szabo,A. (2008) Theory, analysis, and interpretation of single-molecule force spectroscopy experiments. *PNAS*, **105**, 15755–15760.

29. Collin,D., Ritort,F., Jarzynski,C., Smith,S.B., Tinoco,I. and Bustamante,C. (2005) Verification of the Crooks fluctuation theorem and recovery of RNA folding free energies. *Nature*, **437**, 231–234.

30. Greenleaf,W.J., Frieda,K.L., Foster,D.A.N., Woodside,M.T. and Block,S.M. (2008) Direct observation of hierarchical folding in single riboswitch aptamers. *Science*, **319**, 630–633.

31. Woodside,M.T., Behnke-Parks,W.M., Larizadeh,K., Travers,K., Herschlag,D. and Block,S.M. (2006) Nanomechanical measurements of the sequence-dependent folding landscapes of single nucleic acid hairpins. *Proc. Natl. Acad. Sci. U.S.A.*, **103**, 6190–6195.

32. Hunter,W.N., Brown,T., Kneale,G., Anand,N.N., Rabinovich,D. and Kennard,O. (1987) The structure of guanosine-thymidine mismatches in B-DNA at 2.5-A resolution. *J. Biol. Chem.*, **262**, 9962–9970.

33. Allawi,H.T. and SantaLucia,J. Jr. (1998) NMR solution structure of a DNA dodecamer containing single G.T mismatches. *Nucleic Acids Res.*, **26**, 4925–4934.

34. Moe,J.G. and Russu,I.M. (1992) Kinetics and energetics of base-pair opening in 5′-d(CGCGAATTCGCG)-3′ and a substituted dodecamer containing G.T mismatches. *Biochemistry*, **31**, 8421–8428.

35. Allawi,H.T. and SantaLucia,J. Jr. (1998) Thermodynamics of internal C.T mismatches in DNA. *Nucleic Acids Res.*, **26**, 2694–2701.

36. Rossetti,G., Dans,P.D., Gomez-Pinto,I., Ivani,I., Gonzalez,C. and Orozco,M. (2015) The structural impact of DNA mismatches. *Nucleic Acids Res.*, **43**, 4309–4321.

37. Peyret,N., Seneviratne,P.A., Allawi,H.T. and SantaLucia,J. Jr. (1999) Nearest-neighbor thermodynamics and NMR of DNA sequences with internal A.A, C.C, G.G, and T.T mismatches. *Biochemistry*, **38**, 3468–3477.

38. Singh,S., Szulik,M., Ganguly,M., Khutsishvilli,I., Stone,M., Marky,L. and Gold,B. (2011) Characterization of DNA with an 8-oxoguanine modification. *Nucleic Acids Res.*, **39**, 6789–6801.

39. Jang,Y.H., Goddard,W.A. 3rd, Noyes,K.T., Sowers,L.C., Hwang,S. and Chung,D.S. (2002) First principles calculations of the tautomers and pK(a) values of 8-oxoguanine: implications for mutagenicity and repair. *Chem. Res. Toxicol.*, **15**, 1023–1035.

40. Sponer,J., Sponer,J.E., Mladek,A., Jurecka,P., Banas,P. and Otyepka,M. (2013) Nature and magnitude of aromatic base stacking in DNA and RNA: quantum chemistry, molecular mechanics, and experiment. *Biopolymers*, **99**, 978–988.

41. Hoppins,J.J., Gruber,D.R., Miears,H.L., Kiryutin,A.S., Kasymov,R.D., Petrova,D.V., Endutkin,A.V., Popov,A.V., Yurkovskaya,A.V., Fedechkin,S.O. *et al.* (2016) 8-Oxoguanine affects DNA backbone conformation in the EcoRI recognition site and inhibits its cleavage by the enzyme. *PLoS One*, **11**, e0164424.

42. Sanchez,A.M., Volk,D.E., Gorenstein,D.G. and Lloyd,R.S. (2003) Initiation of repair of A/G mismatches is modulated by sequence context. *DNA Repair (Amst.)*, **2**, 863–878.

43. Schibel,A.E.P., An,N., Jin,Q., Fleming,A.M., Burrows,C.J. and White,H.S. (2010) Nanopore detection of 8-Oxo-7,8-dihydro-2′-deoxyguanosine in immobilized single-stranded DNA via adduct formation to the DNA damage site. *J. Am. Chem. Soc.*, **132**, 17992–17995.

44. Kuznetsov,N.A., Koval,V.V., Nevinsky,G.A., Douglas,K.T., Zharkov,D.O. and Fedorova,O.S. (2007) Kinetic conformational analysis of human 8-oxoguanine-DNA glycosylase. *J. Biol. Chem.*, **282**, 1029–1038.

45. Yakovchuk,P., Protozanova,E. and Frank-Kamenetskii,M.D. (2006) Base-stacking and base-pairing contributions into thermal stability of the DNA double helix. *Nucleic Acids Res.*, **34**, 564–574.